

Journal Pre-proof

Optimizing short time-step monitoring and management strategies using environmental tracers at flood-affected bank filtration sites

Janie Masse-Dufresne, Paul Baudron, Florent Barbecot, Philippe Pasquier, Benoît Barbeau



PII: S0048-9697(20)34958-5

DOI: <https://doi.org/10.1016/j.scitotenv.2020.141429>

Reference: STOTEN 141429

To appear in: *Science of the Total Environment*

Received date: 24 April 2020

Revised date: 9 July 2020

Accepted date: 31 July 2020

Please cite this article as: J. Masse-Dufresne, P. Baudron, F. Barbecot, et al., Optimizing short time-step monitoring and management strategies using environmental tracers at flood-affected bank filtration sites, *Science of the Total Environment* (2020), <https://doi.org/10.1016/j.scitotenv.2020.141429>

This is a PDF file of an article that has undergone enhancements after acceptance, such as the addition of a cover page and metadata, and formatting for readability, but it is not yet the definitive version of record. This version will undergo additional copyediting, typesetting and review before it is published in its final form, but we are providing this version to give early visibility of the article. Please note that, during the production process, errors may be discovered which could affect the content, and all legal disclaimers that apply to the journal pertain.

Optimizing short time-step monitoring and management strategies using environmental tracers at flood-affected bank filtration sites

Janie Masse-Dufresne^{a,*}, Paul Baudron^a, Florent Barbecot^b, Philippe Pasquier^a and Benoit Barbeau^a

^a Polytechnique Montréal, Department of Civil, Geological and Mining Engineering, C.P. 6079, succ Centre-ville, Montreal (QC), Canada, H3C 3A7

^b Geotop-UQAM, Chair in urban hydrogeology, Department of Earth and Atmospheric Sciences, C.P. 8888, succ. Centre-ville, Montreal (QC), Canada, H3C 3P8

* Corresponding author.

E-mail addresses: janie.masse-dufresne@polymtl.ca (J. Masse-Dufresne), paul.baudron@polymtl.ca (P. Baudron), barbecot.florent@uqam.ca (F. Barbecot), philippe.pasquier@polymtl.ca (P. Pasquier), benoit.barbeau@polymtl.ca (B. Barbeau).

Abstract: Bank filtration is a popular pre-treatment method to produce drinking water as it benefits from the natural capacity of the sediments to attenuate contaminants. Under flood conditions, bank filtration systems are known to be vulnerable to contamination, partly because flow patterns may evolve at short timescales and result in a rapid evolution of the origin and travel times of surface water in the aquifer. However, high frequency monitoring for water quality is not common practice yet, and water quality management decisions for the operation of bank filtration systems are typically based on weekly to monthly assays. The aim of this study is to illustrate how monitoring strategies of environmental tracers at flood-affected sites can be optimized and to demonstrate how tracer-based evidence can help to define adequate pumping strategies. Data acquisition spanned two intense flood events at a two-lake bank filtration site. Based on bacteriological indicators, the bank filtration system was shown to be resilient to the yearly recurring flood events but more vulnerable to contamination during the intense flood events. The origin of the bank filtrate gradually evolved from a mixture between the two lakes towards a contribution of floodwater and one lake only. Automated measurements of temperature and electrical conductivity at observation wells allowed to detect changes in the groundwater flow patterns at a daily timescale, while the regulatory monthly monitoring for indicator bacteria did not fully capture the potential short timescale variability of the water quality. The recovery to pre-flood conditions was shown to be accelerated for the wells operating at high rates (i.e., ≥ 1000 m³/day), partly because of floodwater storage in the vicinity of the less active wells. These results establish new perspectives to anticipate water quality changes through selected pumping schemes, which depend on and must be adapted to site-specific water quality issues.

Keywords: pumping schemes; quality precursors; environmental tracer; temperature; stable isotopes; electrical conductivity

1 Introduction

Contamination of surface water resources is a worldwide concern (Lopez-Pacheco et al., 2019; Nannou et al., 2020). Many anthropogenic contaminants are routinely detected in rivers and lakes (de Sousa et al., 2014; Glassmeyer et al., 2005; Sjerps et al., 2016; Snyder and Benotti, 2010) and enter watercourses via

Authors' accepted manuscript. Article published in *Science of The Total Environment*, Volume 750, 1 January 2021, 141429. The final published version is available at <https://doi.org/10.1016/j.scitotenv.2020.141429>

© 2020. This manuscript version is made available under the CC-BY-NC-ND 4.0 license <http://creativecommons.org/licenses/by-nc-nd/4.0/>

many diffuse and point sources of contamination (Masoner et al., 2019; Schwarzenbach et al., 2010). For instance, wastewater treatment plants discharge can severely impact the quality of surface waters during droughts (Karakurt et al., 2019). In northern climates, snowmelt periods are particularly critical for combined sewer overflows (Madoux-Humery et al., 2013) and their cumulative effect can rapidly deteriorate the quality of receiving waters from upstream to downstream (Jalliffier-Verne et al., 2016).

Over the last decades, the use of bank filtration (BF) has gained in popularity as a pre-treatment method in regions where surface water resources are threatened by contamination and/or where groundwater resources are scarce (Ahmed and Marhaba, 2017; Tufenkji et al., 2002). BF consists in pumping groundwater from an aquifer which is hydraulically connected to a surface water body. An induced (or natural) hydraulic gradient forces the surface water to infiltrate the banks or bed of a surface water body and eventually reach the pumping well(s). As opposed to direct surface water abstraction, BF systems benefit from the natural capacity of the sediments to attenuate/remove contaminants (Hiscock and Grischek, 2002), including wastewater-derived pathogens (Derx et al., 2013; Lorenzen et al., 2010; Weiss et al., 2005), natural organic matter and xenobiotic organic micropollutants (Bertelkamp et al., 2016; Burke et al., 2014; Dragon et al., 2018; Hamann et al., 2016). However, the efficiency of a BF system to attenuate contaminants depends on numerous parameters, including quality of the surface water (Groschke et al., 2017) and its travel time in the aquifer (Dragon et al., 2018; Hamann et al., 2016).

Under flood conditions, surface water quality is often deteriorated (Whitehead et al., 2009) and short travel times are typically observed at BF systems (Eckert and Irmscher, 2006; Hunt et al., 2005; Wett et al., 2002). As a result, BF systems are vulnerable to pathogens, heavy metal, dissolved organic carbon and organic micropollutant contamination during flood events (Sprenger et al., 2011). Ray et al. (2002) pointed out that small capacity collector wells are less at risk of flood-induced contamination than medium to large capacity collector wells. Ascott et al. (2016) reported high turbidity, organic contaminants, microbial detects, dissolved oxygen and dissolved organic carbon, and low electrical conductivity (EC) during an extreme flood event at a shallow granular aquifer in England. Rose et al. (2018) observed

cyanobacterial contamination due to direct infiltration and damage (i.e., erosion) of the bank during and after a flood event at a river BF site in Australia. BF systems under oxic conditions close to a highly dynamic river were reported to be particularly at risk of contamination under flood conditions, because normally degraded compounds (e.g., diclofenac and bezafibrate) during BF and a significant increase in large cells concentrations were observed in the bank filtrate (van Driezum et al., 2018; van Driezum et al., 2019). BF systems in hilly terrains were also reported to be vulnerable to contamination during flood events (Sandhu et al., 2013). In the province of Quebec (Canada), it is not rare to observe pathogen indicators (such as total coliforms) in municipal pumping wells during springtime freshets, which is perhaps linked to the fact that bank filtration is likely performed unintentionally due to the large density of lakes and rivers, and the close proximity of municipal wells to those waterbodies (Patenaude et al., 2020).

At BF sites, it can be expected that changes of flow patterns and travel times occur at short (e.g., daily) timescales, as demonstrated by Wett et al. (2002). In fact, time-consuming and labor-intensive traditional cultivation-based methods for pathogens analysis are still advocated for routine monitoring of drinking water treatment plants performance (World Health Organization, 2017). As a result, water quality management decisions for the operation of BF systems and post-treatment are typically based on weekly to monthly time-step assays. In addition, Adomat et al. (2020) recently evidenced short timescale bacterial fluctuations during a high temporal resolution monitoring at an ultrafiltration pilot plant and hypothesized a control by rainfall events and/or potential changes in surface water origin. To correctly interpret these variations, the authors highlighted the need to assess for “abiotic” parameters (i.e., EC, pH, dissolved oxygen) which can help to identify the processes controlling microbiological water quality. A promising avenue for providing management strategies would be to anticipate changes in the capacity of bank filtration to attenuate contaminants, driven by the evolution of the origin and travel time of the bank filtrate. Since environmental tracers (i.e., temperature, EC and $\delta^{18}\text{O}$) have been shown to be good proxies for these two parameters (Baudron et al., 2016; des Tombe et al., 2018; Massmann et al., 2008; Vogt et al.,

2010), the analysis of their evolution could provide an improved understanding for the management of bank filtration sites.

The aim of this study is to illustrate how monitoring strategies of environmental tracers at flood-affected sites can be optimized and to demonstrate how tracer-based evidence can help to define adequate pumping strategies. We performed a tracer monitoring which covered two intense flood events at a two-lake bank filtration site. It was conducted at various sampling locations (i.e., pumped mix, pumping wells and observation wells) and time-steps (i.e., from sub-daily to monthly), while bacterial sampling was conducted at a monthly time-step. By doing so, it was possible to better understand the timescales of changes in the groundwater flow patterns and, thus, anticipate the water quality dynamics. The comparison of the information provided by the different sampling locations allows discussing the representativity and relevance of environmental tracers and standard bacteriological analysis. Their contribution to the pumping strategies for real-time water quality management is then depicted.

2 Study site description

2.1 Hydrological and geological contexts

The studied lake-BF system is located in a peri-urban region in the south of the province of Quebec, Canada (Figure 1a). A total of 8 pumping wells were installed in a small fully unconfined aquifer of approximately 500 m wide and 120 m long and with a maximum thickness of 26 m. Ageos (2010) described this aquifer as a buried valley carved into the Champlain Sea clays (Figure 2). The aquifer is mainly composed of alluvial fine to medium sands and has a hydraulic conductivity of 2.7×10^{-3} m/s (Ageos, 2010). A small lens of alluvial gravel is also found at the bottommost part of the aquifer in the vicinity of P4 and P5. The topography of the study area is nearly flat, with minimum and maximum observed surface elevations of 23.76 m.a.s.l. and 27.91 m.a.s.l. (Ageos, 2010). On the North-East and South-West limits of the aquifer are two artificial lakes, namely Lake A and Lake B which were created from sand dredging activities.

The pumping wells are all screened at the base of the aquifer over 8 m long sections, except for P5 which has a 4 m long section. The screened sections of the observation wells PZ-2, PZ-5 and PZ-6 are also located at the bottom of the aquifer and over 9 m, 3 m and 6 m, respectively. No information is available concerning the design of the observation well PZ-4. The pumping wells receive water from Lake A and Lake B and no contribution from regional groundwater was identified. The mixing ratio between Lake A and Lake B waters range from 0% to 100% and is influenced by the pumping rate and the water level difference between the lakes. During springtime, the contribution from Lake A tends to be > 50% at all pumping wells (Masse-Dufresne et al., 2019). A numerical groundwater flow model was previously developed by Ageos (2010) and the mean travel times were estimated as 2 days from Lake B and 10 days from Lake A.

Lake A is an exploited and flooded sandy pit of approximately $2.8 \times 10^5 \text{ m}^2$ and has a maximal observed depth of 20 m. It receives surficial inflow from a small stream (S1) with an annual mean discharge of $0.32 \text{ m}^3/\text{s}$ (Ageos, 2010). Surficial outflow fluxes via a 1 km long channeled stream (S2) can only occur given a sufficiently high water level, due to a topographic threshold at 22.12 m.a.s.l. (Ageos, 2010). The direction of water fluxes at S2 can be reversed when the water level of Lake DM is exceeding both the topographic threshold and the one of Lake A (see arrows on Figure 1b). Such conditions lead to surficial inputs from Lake DM, resulting in a hydraulic connection with a large watershed as the latter corresponds to a widening of the Ottawa river (Figure 1a). Subsurface water fluxes between Lake DM and Lake A are not likely, since impervious sediments (i.e., Champlain Marine Clays) are underlying the thin layer of alluvial sands (i.e., only few metres) between Lake A and Lake DM (Ageos, 2010). Lake B is a former sandy pit of approximately $7.6 \times 10^4 \text{ m}^2$ with maximum observed depth of 19 m. It is nowadays surrounded by residential area and a public recreational beach. It has no surficial inlet and is thus mainly fed by precipitations and groundwater. An artificial surficial outlet (at approximately 21.8 m.a.s.l.) can drain Lake B water towards the town's stormwater collection system

2.2 Flood-proof measures

All the pumping wells are equipped with a subsurface well chamber (in concrete) in which automatic pumps drain water that can infiltrate due to precipitations, snowpack melting and/or rising of the water table. Note that during normal hydrological conditions, the water table is below the well chambers. During intense flood events, temporary headworks are erected around the pumping wells to prevent infiltration of floodwater into the well chamber from the surface. Concerning the observation wells, steel casings prevent direct infiltration of floodwater.

2.3 Operation of the BF system

A schematic illustration of the BF system and treatment plant is shown in Figure 3. All the pumping wells are equipped with a variable flow submersible pump, except for P5 which has a fixed flow pump. When a well is abstracting water, the raw water can flow either towards a purging system or towards the treatment plant, accordingly to the position of the valves and the needs of the waterworks. All the active pumping wells contribute to the pumped mix, which is further treated and chlorinated before its distribution to the drinking water supply system.

The total pumping rate ranges between 4000 m³/day and 7500 m³/day. The pumping wells P3 and P6 are typically contributing the most to the pumped mix and are continuously operated at ≥ 1000 m³/day. During the daily peak demand and/or the summertime, P1, P2, P7 and P8 are operated intermittently (i.e., few hours per day). Lastly, P4 and P5 are only occasionally in operation (i.e., few minutes to hours per month). Further details concerning the pumping schemes are available in a previously published work (Masse-Dufresne et al., 2019).

3 Materials and Methods

3.1 Instrumentation

Lake A, Lake B and observation wells (i.e., PZ-2, PZ-4 and PZ-6) were equipped with pressure-temperature data loggers (Divers®, micro-Diver, Van Essen Instruments, Delft, Netherland). The loggers were installed at roughly 10 m to 12 m depth below the ground level in all three observation wells. PZ-2

was additionally equipped with a pressure-temperature-EC data logger (Divers®[®], CTD-Diver, Van Essen Instruments, Delft, Netherland) which was installed at 20 m depth below the ground level and in front of the screened section of the observation well. All measurements were done on at a 15 min to 30 min time-step. A barometer (Divers®[®], micro-Diver, Van Essen Instruments, Delft, Netherland) was also installed on-site to perform the barometric compensation (for the calculation of water level from pressure measurements). Accuracy for pressure, temperature and EC measurements were ± 1 cmH₂O, $\pm 0.1^\circ\text{C}$ and ± 10 $\mu\text{S}/\text{cm}$, respectively. It is assumed that the EC measurements at PZ-2 (at 20 m depth) are representative of groundwater in its vicinity, since the level logger was placed in front of the screen, where water enters and exits the piezometer according to the existing groundwater flow. It is also assumed that temperature measurements at the observation wells (at 10-12 m and 20 m) are representative of the adjacent groundwater conditions.

Mean daily water levels at Lake DM were obtained with permission from the *Centre d'Expertise Hydrique du Québec* database (Centre d'Expertise Hydrique du Québec, 2020). Daily means (for water levels, temperature and EC measurements) were calculated in order to produce consistent time series. Precipitations from Mirabel International Airport, i.e., the closest meteorological station (18 km from the study site), were retrieved from Environment and Climate Change Canada database (available online at weatherstats.ca).

3.2 Water sampling and analytical procedures

Water sampling was performed on a weekly to monthly basis at the surface of Lake A, Lake B and at the pumping wells (P1 to P8) following the procedure described in Masse-Dufresne et al. (2019). During the 2017 and 2019 springtime flood events, additional sampling campaigns were conducted. In 2017, additional measurements and water samplings were performed at observation wells (i.e., PZ-2, PZ-4 and PZ-5) at a weekly to monthly timestep. In 2019, the raw pumped mix was sampled by the operators of the drinking water facility on a daily basis at a by-pass faucet, prior to treatment for potabilization, in order to perform measurements of EC and analyses of $\delta^{18}\text{O}$ and $\delta^2\text{H}$. Note that access to the pumping wells and the

pumped mix sampling point was not restricted during the flood events. As stated in section 2, automatic pumps drain water that can infiltrate in each well chamber, which enables sampling of the pumping wells year-round. Also, the sampling point for the pumped mix is in the water treatment plant building and is therefore easily accessible, even during flood events.

High-density polyethylene (HDPE) 60 mL bottles (Thermo Scientific™ Nalgene™ Narrow-Mouth HDPE Economy Bottles, Rochester, New York, United States) were used to collect samples for $\delta^{18}\text{O}$ and $\delta^2\text{H}$ analysis, which were stored at room temperature. Filtration through a 0.45 μm hydrophilic polyvinylidene fluoride (PVDF) membrane (Millex-HV, Millipore, Burlington, MA, USA) was performed in the laboratory when needed. Analyses for stable isotopes of water were performed with a Water Isotope Analyzer with off-axis integrated cavity output spectroscopy (LGR-T-LWIA-45-EP, Los Gatos Research, San Jose, CA, USA) at Geotop-UQAM laboratory (Montreal, Quebec). Three internal reference standards ($\delta^{18}\text{O} = -6.71\text{‰}$, -4.31‰ and -20.31‰ ; $\delta^{17}\text{O} = -7.23\text{‰}$, -2.31‰ and -19.96‰ ; $\delta^2\text{H} = -51.0\text{‰}$, -25.19‰ and -155.40‰) calibrated on the VSMOW-SLAP scale were used to correct the data. The analytical uncertainty (1σ) is 0.15‰ and 1‰ for $\delta^{18}\text{O}$ and $\delta^2\text{H}$, respectively.

4 Results and discussion

4.1 Long-lasting hydraulic control by floods

4.1.1 Recurrent and extreme events

During springtime and autumn, water level at Lake DM normally rises due to snowpack melting and/or precipitations over the watershed. From 1987 to 2016, mean water levels of Lake DM in April and May are 22.82 m.a.s.l. and 22.51 m.a.s.l., respectively (Centre d'Expertise Hydrique du Québec, 2020), which is higher than the topographic threshold (at 22.12 m.a.s.l.). In fact, water level rise at Lake DM induces a yearly recurrent hydraulic connection with Lake A and allows for floodwater inputs (from Lake DM) to Lake A, typically from April to May (Ageos, 2016).

The evolution of water levels at Lake DM from 2014 to 2020 is represented in Figure 4a. For normal hydraulic conditions, the total duration of the flood events is typically between 80 and 95 days and the maximum water level rise above the threshold is 1.5 m. In 2017 and 2019, springtime water level rise at Lake DM was particularly important (i.e. > 2.6 m above the topographic threshold) and the flood events lasted 150 days and 106 days, respectively. Unprecedented historical water levels (i.e., 24.77 m.a.s.l. and 24.75 m.a.s.l.) were reached on May 8, 2017 (Figure 4b) and April 29, 2019 (Figure 4d). Note that there was no risk of direct infiltration of floodwater into the pumping wells and the observation wells (see section 2.2) in 2017 and 2019, except for PZ-6 (in 2017 only) where the elevation of the steel casing is at 24.78 m.a.s.l., which is similar to the maximal water level at Lake DM (i.e., 24.77 m.a.s.l.). On the other hand, the area in the vicinity of PZ-6 was inundated in 2017 and 2019 (see Figure 1c) and short-circuiting of floodwater along the steel casing could have potentially occurred at PZ-6.

In 2017 and in 2019, the temporal evolution of water levels at Lake A, Lake B and PZ-4 are mainly showing similar trends as Lake DM, indicating a control of Lake DM over the water levels of the whole hydrosystem during the springtime flooding (Figure 4b and d). In 2018, the water level at PZ-4 is also governed by the fluctuation of Lake DM when the latter exceeds the topographic threshold (Figure 4c). These results suggest that Lake A receives floodwater inputs from Lake DM during both recurrent and extreme flood events.

4.1.2 Dyke failure

To prevent inundation of inhabited areas, numerous municipalities surrounding Lake DM have built dykes. However, in April 2019, the important water level rise at Lake DM caused a dyke to fail at approximately 1 km eastwards from the study site, resulting in the flooding of a residential area (including Lake B) and forcing the evacuation of 6,000 people. Comparison between the extent of the flooded areas in 2017 and 2019 (Figure 1b) suggest that the dyke failure imposed different hydraulic conditions to the BF system. In fact, it caused an important water level rise at Lake B and PZ-4 (Figure 4d). The town authorities rapidly proceeded to (i) the construction of temporary dykes to constrain the flooded area and

(ii) the installation of a pumping station at Lake B, which allowed to artificially lower the water levels at Lake B and PZ-4.

4.2 Water quality risk assessment

4.2.1 Spatiotemporal variability of coliform counts at the pumping wells

A regulatory microbiological water quality monitoring is performed monthly at all the pumping wells. Included in this routine monitoring are the standard culture-based analysis for total coliforms, which also includes the atypical counts (i.e., the colonies which do not produce a green shine on the m-Endo media), and for *E. coli*.

Figure 5 illustrates the spatiotemporal evolution of total counts on m-Endo media (sum of atypical and typical colonies) at the pumping wells from 2014 to 2019. Note that all analyses for *E. coli* were negative during the same period. Total counts at all the pumping wells are typically < 1 CFU/100 ml and, occasionally, ≥ 1 CFU/100 ml and < 10 CFU/100 ml. Bacterial detects are rarely summing > 10 CFU/100 ml, and if so, it is only occurring at one single pumping well, except during the extreme flood events. In May 2017, the bacterial detects were positive at all the pumping wells and $> 60\%$ (5/8) of the pumping wells showed ≥ 10 CFU/100 ml and < 100 CFU/100 ml. A similar pattern, but with less important bacterial detects, was observed during the 2019 flood event. Considering the above, the bank filtration system appears to be resilient to the yearly recurring flood events but more vulnerable to contamination during the intense flood events (such as 2017 and 2019).

4.2.2 Tracking the origins of coliform bacteria

The quality of the Ottawa River (i.e., the discharging waters to Lake DM) is known to be altered by the contamination from combined sewage overflows (Jalliffier-Verne et al., 2016) and was particularly affected during the studied flood events (CBC News, 2017). Water quality of Lake DM was thus very likely to be affected by combined sewage overflows occurring at the watershed scale, which can be a source of wastewater-derive pathogens, including total coliforms. As Lake A receives floodwater inputs

from Lake DM during springtime, wastewater-derived contamination is a potential threat to the BF system.

However, total coliforms are ubiquitous in the environment and are thus not only sourced from fecal origin (Glassmeyer et al., 2005; Martin et al., 2010). Rainfall events can lead to the transport of pathogens initially present in soils, resulting in the pollution of receiving waters (Frey et al., 2015). Precipitations were particularly important in 2017 and 2019, as the cumulated precipitation (as rain and/or snow equivalent) from January to May summed at 578 mm and 498 mm, while it was ranging from 330 mm to 418 mm for the other years (Figure A1). Moreover, the 2017 and 2019 springs are characterized by more heavy and consecutive rainfalls. Given the intensity of rainfalls along with the snowpack melting during springtime in 2017 and 2019, it is also likely that endogenous bacteria to the sediments were detected at the pumping wells due to water level rise and evolution of the prevailing groundwater flow patterns. Although the presence of total coliforms is not strictly indicative of fecal contamination, the increase in bacterial counts during the two intense flood events (i.e., 2017 and 2019) are still indicative of a change in the hydrological process and/or flow patterns which affects the origin of the pumped water.

4.3 Groundwater flow dynamics: from normal to flood conditions

This section aims at studying the evolution of the origin of the bank filtrate due to the 2019 intense flood event, in order to better understand the groundwater flow dynamics. To do so, the evolution of EC and $\delta^{18}\text{O}$ at short timescale (daily) at the pumped mix is examined. Then, the origin of the bank filtrate at the pumping wells and at a monthly time-step from January 2017 to June 2019 is assessed in order to discuss the representativity of the interpretations derived from monitoring at the pumped mix.

4.3.1 Temporal evolution of EC and $\delta^{18}\text{O}$ at the pumped mix

The pumped mix corresponds to the raw pumped water from multiple wells, which is further treated and chlorinated before its distribution to the drinking water network (see Figure 3). Sampling of the pumped

mix was efficiently performed daily by the plant operators during springtime and summer 2019 to cover the flood event and the recovery to normal conditions.

Figure 6 depicts the temporal evolution of EC and $\delta^{18}\text{O}$ at the pumped mix, which is discretized in three periods. The evolution of $\delta^2\text{H}$ (data not shown) was found to be very similar to $\delta^{18}\text{O}$, which suggests that both stable isotopes of water ($\delta^{18}\text{O}$ and $\delta^2\text{H}$) are illustrating the same processes. Therefore, no discussion concerning $\delta^2\text{H}$ is provided. First, normal hydraulic conditions were prevailing in early April. The observed EC was $685 \mu\text{S}/\text{cm}$ at the pumped mix. In comparison, mean Lake A and Lake B EC values are $500 \mu\text{S}/\text{cm}$ and $800 \mu\text{S}/\text{cm}$, respectively. As it was demonstrated in previous work, this indicates that the pumped water was a mixture between Lake A and Lake B waters (Masse-Dufresne et al., 2019). Then, under flood conditions, a decreasing trend for both tracers was observed over a 1-month period (from April 15 to mid-May) as shown in Figure 6. The EC evolution indicates that the pumped water transitioned from a mix between Lake A and Lake B to exclusively Lake A water during the flood event. Considering that floodwater is characterized by a depleted signature in heavy isotopes (mean value of -11.7‰), it appears as a good proxy to denote the presence of floodwater. Depleted signatures (i.e. $< -12 \text{‰}$) were observed at the pumped mix during a two-week period around mid-May, suggesting that the bank filtrate was particularly influenced by the flood-marked water. Finally, in late May, EC and $\delta^{18}\text{O}$ recovered towards initial values over a two-month period. This result suggests that when the water level at Lake DM exceeds the topographic threshold (at 22.12 m.a.s.l.), the latter has a decisive impact on the origin of the pumped water.

In early May, the observed EC and $\delta^{18}\text{O}$ values tended to slightly deviate from the expected curve (Figure 6b). This is very likely due to the above-mentioned failure of the dyke (see section 4.1.2; Figure 4d), which resulted in a rapid evolution of the water level difference between Lake DM (and Lake A) and Lake B. Another potential controlling factor is a change in the pumping scheme, as P3 was out of operation from April 29 and P7 (or occasionally P8) was activated to maintain the needed daily pumped volume. In either case, this result denotes the important reactivity of the BF system to changes in

hydraulic conditions, and thus suggests that the travel times of water to the pumping wells are short. However, monitoring for environmental tracers at the pumped mix has limitations. In fact, no precise estimation of travel times can be done with this dataset since it is composed of abstracted water from different wells.

4.3.2 Spatiotemporal variability of EC and $\delta^{18}\text{O}$ at the pumping wells

Given the potential spatial heterogeneity of the hydrogeological parameters and the variability of the pumping rate at each well, it is expected that there is a spatial variability in the evolution of the flow patterns along the BF system. This raises questions concerning the representativity of the evolution of the origin of water in the pumped mix. This subsection aims at exploring such question by confronting the interpretations derived from monitoring at the pumped mix (last subsection) to interpretations derived at a higher spatial resolution, i.e., at each pumping well.

Figure 7 depicts the monthly evolution of EC and $\delta^{18}\text{O}$ at the pumping wells from March 2016 to June 2019. For each sampling campaign, a boxplot illustrates the distribution of the environmental tracers at the sampled pumping wells (i.e., up to 8). For comparison purposes, representative values for Lake A and Lake B or for floodwater are also illustrated.

Under normal hydraulic conditions, there is typically a large variability of the two tracers at each pumping well. For instance, the EC can range between mean Lake A (i.e., 506 $\mu\text{S}/\text{cm}$) and mean Lake B (i.e., 802 $\mu\text{S}/\text{cm}$) values for a single sampling campaign. This observation demonstrates that the groundwater flow patterns are normally heterogenous along the BF system. In contrast, all the pumping wells tend to converge towards floodwater and Lake A water types during the flood events, suggesting a common forcing on the origin of the bank filtrate. Since the same trends were observed at all the pumping wells during the flood events, interpretations derived from monitoring at the pumped mix can be extrapolated to the whole BF system. More precisely, the dynamics of the origin of water to the pumping wells contributing to the pumped mix also apply to the less active pumping wells under flooding

conditions. However, the transition to a homogeneous behavior was not detected as it occurred between two sampling campaigns, i.e., within a one-month period. Hence, based only on the EC and $\delta^{18}\text{O}$ variations we infer that the travel time of the bank filtrate during the flood events is < 1 month.

Additionally, it appears that the intensity of the flood event drives the amplitude of the EC and $\delta^{18}\text{O}$ shifts. In fact, for the 2016 and 2018 flood events, EC values remained higher than the mean Lake A value at the pumping wells. Concerning the isotopic composition, depleted values (< -11.5 ‰, i.e., mean floodwater value) were only observed during the more intense flood events (2017 and 2019). Hence, the isotopic composition is proven to be useful due to its specificity to depict significant floodwater contribution and, consequently, differentiate between the recurrent yearly floods and the extreme events at this study site. Also, a tardy recovery to initial values is observed at some wells for the 2017 intense flood event, suggesting potential flood water storage which is likely influenced by the pumping rates. Further discussion on this topic is provided in section 4.5.2.

4.4 Temperature as a proxy of transient groundwater flow patterns during flood events

The combined use of EC and $\delta^{18}\text{O}$ was proven to be adequate to track the origin of the pumped water. When such monitoring is applied to the pumped mix or the pumping wells, it is, however, not possible to gain insights into the travel times of the bank filtrate which is of utmost importance for water quality risk management. In this section, we develop an interpretative framework of the behavior of temperature which helps at understanding timescales and the timing of the impacts of flood events on the groundwater flow pattern.

Figure 8 illustrates the temporal evolution of temperature at PZ-6 (distant from the BF system) and vertical temperature profiles at two observation wells (PZ-2 and PZ-5) along the BF system during normal hydraulic conditions (March 19, 2019) and flood conditions (April 25, 2019). Observation well PZ-6 is located southeastwards from the BF system (see Figure 1). In that area, the groundwater flow pattern is believed not to be influenced by the pumping. Surface water from Lake A infiltrates the bank and flows

towards Lake B, as the water level of Lake A is higher than Lake B. Electrical conductivity at PZ-6 (476 $\mu\text{S}/\text{cm}$; in September 2018) also supports this interpretation. A similar flow pattern is expected at PZ-5, as the latter is located near pumping well P5, which is only rarely abstracting water (i.e., 1-2 hours for the regulatory monthly monitoring). On the other hand, observation well PZ-2 is located between Lake B and the pumping well P1 (continuously pumping). Under normal hydraulic conditions, surface water from Lake B infiltrates the sandy bank and eventually reaches pumping well P1. Thus, the groundwater in the vicinity of PZ-2 is normally originating from Lake B and physicochemical parameters are governed by the conditions at Lake B. Hence, it can help at understanding the dynamics of temperature under the influence of pumping.

As shown in Figure 8a, from September 2018 to late February 2019, the temperature measured at PZ-6 increased gradually (up to 17°C), while it was decreasing (down to 4°C) at Lake A. Under flood conditions, temperature at PZ-6 decreased rapidly, and low temperatures ($< 2^\circ\text{C}$) were observed in late April. Similarly, a decrease of the temperatures also occurred at PZ-5 (Figure 8c). At PZ-2, the temperature ranged from 1°C to 5°C on March 19, 2019 (Figure 8b). Such cold temperatures are resulting from the infiltration of cold water from Lake B during wintertime. Then, under flood conditions, a rapid warming of groundwater was observed at PZ-2 (Figure 8b).

To summarize, the flood event has significantly altered the temperature dynamics at the observation wells and the vertical temperature profiles (at PZ-2 and PZ-5) seem to converge towards 10°C. Based on the available data, it is not possible to conclude on the origin of this 10-degree water. It is potentially corresponding to the floodwater. However, as the mean air temperature was mainly $< 10^\circ\text{C}$ until early May (see Figure A2), we expected that the floodwater temperature would be lower than 10°C. Besides, the flood event modified the prevailing groundwater flow pattern and likely triggered the mobilization of a warm groundwater which could have mixed with cold and recently infiltrated water from Lake A. Such scenario would have resulted in the observed 10-degree water at both observation wells PZ-2 and PZ-5, but further research is still needed to test this hypothesis.

In addition, daily time-step measurements of temperature and EC were performed at PZ-2 (Figure 9), in order to gain further insights into the timescales and the timing of the flood event impacts on the groundwater flow in the vicinity of the pumping wells. Only continuous measurements of water levels, temperature and EC were performed, due to robustness and practicality of those measurements.

From late March to mid-April, normal hydraulic conditions were prevailing, and the observed temperatures and EC were nearly constant (Figure 9a). In mid-April, temperature at 11 m depth, and to a lesser extent at 20 m, started to decrease (Figure 9b). This temperature change coincides with the timing of the EC decrease and $\delta^{18}\text{O}$ depletion at the pumped mix (see Figure 6). On April 23, a rapid increase of temperature was observed at both depths. In the meantime, EC values rapidly decreased and plateaued at 500 $\mu\text{S}/\text{cm}$ in late April (Figure 9a), suggesting that the origin of the water at PZ-2 transitioned from Lake B to Lake A water within a 1-week period. The hydraulic gradient between Lake B and PZ-2 is coherent with this interpretation (Figure 9b). Then, a rapid decrease of the temperature at 11 m and 20 m was observed (starting on April 25, 2019) and temperatures $< 5^\circ\text{C}$ were reached within a 2-day to 3-day period. As EC remained approximately 500 $\mu\text{S}/\text{cm}$, this is evidencing the existence of short travel times between Lake A and PZ-2, which are of major concern for the evolution of water quality at bank filtration sites (Sandhu et al., 2018).

A repetition of this pattern (i.e., temperature increase-decrease) was observed immediately following the dyke failure (Figure 9b). This possibly led to the remobilization and “back-flow” of the warmer groundwater, as an inversion of the hydraulic gradient was observed (Figure 9b). Again, constant EC values (at 500 $\mu\text{S}/\text{cm}$) suggest that this remobilized warm water originated from Lake A. As mentioned in the section 4.3.1, a change in the pumping scheme also occurred shortly after the dyke failure, and the activation of pumping well P8 (next to P1) could also have influenced the groundwater patterns in the vicinity of PZ-2.

The observed dynamics of the temperature at PZ-2, PZ-5 and PZ-6 indicate that the flood event led to a reorganization of the groundwater flow patterns between Lake A and Lake B. Indeed, the flood event

could have forced the vertical infiltration of cold water and/or a horizontal mobilization of cold water from Lake A due to increased hydraulic gradients across the sandy bank. It is, however, not possible to differentiate between the two processes and thermo-hydrodynamic modeling would be needed to conclude on the origin of the cold water. Yet, it was demonstrated that a descriptive interpretation of temperature, combined with the evolution of water levels and EC, can depict the timescales and timing of the impact of flood events on the groundwater flow pattern.

4.5 Water quality management implications

4.5.1 Optimizing monitoring strategies with low-cost precursors of water quality changes

When comparing the timescales of groundwater flow dynamics to the frequency of bacterial analyses sampling (see black asterisks in Figure 9a), it becomes clear that contamination events may occur between the monthly regulatory monitoring. The current strategy is therefore not adequate for the surveillance of microbiological water quality at this BF system under flood conditions. Moreover, the analytical delay for standard cultured-based analysis is typically 24 h to 48 h, to which is to be added the transport of the samples to the laboratory. In total, it can take up to three days from sample collection to delivery of the analytical result (see gray shaded areas in Figure 9a). Under flood conditions, the origin and travel times of the water at BF sites are subject to evolve at a much shorter timescale (i.e., within a 1-day period), as evidenced by the evolution of temperature and EC in figure 9a. In summary, discrete sampling for microbiological assays at the pumping wells and/or the pumped mix is only representative of a “snapshot” in time and most probably in space, and water quality management decisions based on a monitoring at a monthly time-step may not represent the full picture and may lead to misinformation.

High frequency monitoring of microbiological water quality is not yet common practice. Near real-time monitoring technologies for the detection of microbial indicators via fluorescence-based methods, such as flow cytometry (Clausen et al., 2018) or enzymatic activity (Burnet et al., 2019), are in development and might in the future provide additional information at a proper timescale. Adomat et al. (2020) assessed the

biomass dynamics at high resolution at three BF sites via flow cytometry and enzymatic detection methods. While such monitoring was shown to enhance the understanding of microbiological dynamics of the treated water at BF sites, they reported some divergence between the results due to methodological limitations. Some practical disadvantages (e.g., cost, maintenance, no species differentiation) are also presently limiting the widespread implementation of high frequency monitoring technologies of biomass (Zamyadi et al., 2016).

Despite the worldwide application of managed aquifer recharge techniques, which include BF systems, management guidelines are limited to few examples, and field-scale studies are still needed to improve design, operation and maintenance of existing and future sites (Dillon et al., 2019). Indeed, the operation and management of most BF systems are based on practical knowledge derived from past applications (Ahmed and Marhaba, 2017). Hydrogeochemical conceptual models are developed according to site-specific hydrogeological (e.g., water levels, porosity, hydraulic conductivity) and geochemical data (e.g., quality of surface water and groundwater, redox conditions) in order to characterize the general performance of a BF system and to determine the operational pumping rates. Depending on the spatio-temporal resolution of the assessments, the representativity of hydrogeochemical models may be limited and only informative of the baseline trends. Sprenger et al. (2011) highlighted that prediction tools to assess the risk of contamination under extreme hydraulic conditions (i.e., floods and droughts) are particularly needed. Measurement of robust and low-cost parameters, such as EC and temperature, are part of the routine monitoring strategy at a number of existing BF systems and it is worth using these parameters as management tools. Monitoring of turbidity is also common at many BF sites. For instance, Ascott et al. (2016) studied the evolution of the turbidity over a 6-month period, which spanned over an extreme flood event, at a river-BF site along the Thames (England). While the turbidity of the river fluctuated between roughly 5 NTU and 50 NTU, the turbidity of the pumped water remained < 0.5 NTU for all the study period, except during the flooding of the ground surface. During this period, the turbidity of the pumped water reached up to 1.5 NTU. Ascott et al. (2016) suggested that the increase of the

turbidity indicated a rapid vertical infiltration of floodwater, while the reduction in turbidity (river vs. bank filtrate) testified that the attenuation processes were still occurring and help at maintaining the quality of the bank filtrate. Hence, turbidity monitoring is valuable as it can serve as a dual indicator for (1) the development of rapid flow paths and (2) the resilience of the BF system to flood events.

In the previous sections, it was demonstrated that monitoring for environmental tracers at a short time-step fully captures the transience of groundwater flow paths at the BF system, as it allowed to track the evolution of the origin and residence time of the bank filtrate in near real-time. Hence, monitoring for environmental tracers can help at better understanding the vulnerability to microbiological contamination. For instance, in the studied case, monitoring for EC was shown to be useful to detect changes in mixing ratios (between Lake A and Lake B), while $\delta^{18}\text{O}$ helped to decipher the contribution of floodwater to the bank filtrate. By combining high frequency monitoring for EC and $\delta^{18}\text{O}$, changes of the origin of the bank filtrate were detected in real-time. Assuming that the quality of the water sources to the pumping wells are different, knowledge of the origin of water is crucial to anticipate water quality changes of the bank filtrate.

Monitoring for temperature was shown to depict the local flow heterogeneity and can be used as an early warning tool for potential evolution of the travel times. Since shorten travel times (and/or shorten travel distances) may lower the performance of BF systems to attenuate pathogens (Sprenger et al., 2011), such information is of paramount importance for the understanding of the vulnerability to microbiological contamination. A comprehensive review of the use of temperature as a tracer is provided in Anderson (2005) and states that its applicability is limited to contexts where there is a marked contrast between surface water and groundwater. Other environmental tracers, such as radon (Gilfedder et al., 2019), would be suited to depict the transience of BF systems in other contexts, where temperature is less adequate.

Considering the above, monitoring for environmental tracers provides guidance for optimizing the timing and the frequency of more expensive and time-consuming monitoring analyses (e.g., pathogens or trace organic contaminants). Besides, monitoring for environmental tracers at the pumping wells and/or the

pumped mix can provide crucial insights for the implementation of near real-time evidence-based preventive measures in order to secure the quality of the drinking water while regulatory water quality analyses are awaited.

4.5.2 Towards a control of the bank filtrate quality through modulated pumping schemes

Based on the data at the pumping wells, it was demonstrated that there is a spatial variability of the groundwater flow pattern under normal hydraulic conditions (section 4.3.2). Hence, it was suspected that the recovery at each single well could vary from the one of the pumped mix, due to the variability of the pumping rates. A selection of two to four wells are normally contributing to the pumped mix on a daily basis and they operate at a daily pumping rate $Q \geq 1000 \text{ m}^3/\text{day}$, while the other three wells are rarely active. This selection is typically consistent on the long-term, but changes may occur if a well is out of operation due to a pump failure for instance.

Figure 10 shows the evolution of $\delta^{18}\text{O}$ at the pumping wells during the recovery period in 2017. It illustrates that the recovery at the wells contributing to the pumped mix (i.e., $Q \geq 1000 \text{ m}^3/\text{day}$; in black) is more rapid than for the other wells. The isotopic signature of the more active pumping wells plateaued at approximately -10.25 ‰ in late July, suggesting a complete recovery. Besides, from mid-May to early August 2017, pumping well P3 was out of operation. When it started pumping again in August, $\delta^{18}\text{O}$ was relatively depleted and similar to the observed isotopic signature during the flood event, suggesting a significant contribution from flood-marked water, which was likely stored in the bank in the vicinity of P3. These results suggest that high pumping rates ($Q \geq 1000 \text{ m}^3/\text{day}$) accelerated the recovery in comparison to lower pumping rates. Also, bank storage of flood-marked water was possible in the vicinity of the less active pumping wells. This water could have been pumped by the wells more than three months after the flooding.

These results establish new perspectives to control the origin of the bank filtrate and anticipate water quality changes through modulated pumping schemes. Monitoring and surveillance strategies will

naturally depend on site-specific water quality issues. Hereafter are presented two examples of management strategies considering that wastewater-derived contamination were transported by floodwater. Firstly, one could attempt to increase the travel time in order to limit the development of rapid flow paths. This strategy would help maintain the efficiency of the BF system in attenuating the contaminants by simply distributing the total pumping rate over all the available pumping wells prior and during the flood events. Secondly, given that some wastewater derived contaminants are persistent in the water cycle (Reemtsma et al., 2016), bank storage of surface water could pose a threat for the quality of the bank filtrate during few months. In fact, if the surface water were hypothetically polluted with persistent contaminants (during a flood event or not), persistent contaminants could potentially be found in the bank filtrate event after the remediation of the surface water quality. Hence, when reactivating a pumping well, it would be possible to rapidly purge the stored water by pumping at high rates. Note that the purged water is not to be distributed in the drinking water supply system, but rather flushed to an adjacent urban runoff collector. Overall, the monitoring of environmental tracers at the pumping wells and pumped mix would help at defining such pumping strategies and appreciate the impacts of a pumping scheme modification in real-time.

5 Conclusions

In this study, we illustrated how monitoring strategies of environmental tracers at a flood-impacted BF site can be optimized to better understand the timescales of changes in the groundwater flow patterns and anticipate the water quality evolution. This knowledge provides key information to improve existing operational strategies through modulated pumping sequences.

Based on bacteriological indicators (total coliforms), the BF system was shown to be resilient to the yearly recurring flood events but more vulnerable to contamination during the intense flood events (such as 2017 and 2019). The evolution of EC and $\delta^{18}\text{O}$ at the pumped mix and at the pumping wells revealed that the hydraulic connection with a large watershed has a decisive impact on the groundwater flow patterns at the BF system. Under flood conditions, the origin of the bank filtrate gradually evolved from a mixture

between Lake A and Lake B waters towards a contribution from Lake A and Lake DM (i.e., floodwater) only. Additionally, monitoring for environmental tracers allowed to track the impact of a dyke failure on the origin of the bank filtrate, and revealed the rapid reactivity of the BF system.

Automated measurements of temperature and EC at observation wells allowed to detect changes in the groundwater flow patterns at a daily timescale, while the regulatory monthly monitoring for microbiological water quality did not fully capture the potential short timescale variability of the water quality. Hence, real-time monitoring of environmental tracers at observation wells can be seen as early warning tools to anticipate potential changes in the water quality of the bank filtrate.

The recovery of the BF was accelerated for the wells operating at high rates (i.e., $\geq 1000 \text{ m}^3/\text{day}$) in comparison to the other wells, partly because of floodwater storage in the vicinity of the less active wells. These results establish new perspectives to control the origin of the bank filtrate and anticipate water quality changes through selected pumping schemes, which depend on and must be adapted to site-specific water quality issues.

In summary, the monitoring of environmental tracers at BF sites should be performed at different observation points in order to anticipate water quality changes and, thus, provide guidance for optimizing the timing and the frequency of more expensive and time-consuming monitoring analyses (e.g., pathogens or trace organic contaminants). Monitoring for environmental tracers can help to optimize and perform real-time surveillance of the pumping schemes strategies. However, field-scale experiments are still needed to test the application of such monitoring and pumping strategies and evaluate their effectiveness in controlling the quality of the pumped water.

Conflict of interest

None.

Acknowledgments

The authors gratefully acknowledge the Town for their financial support and for their help in the field. This research was also funded by NSERC [grant numbers CRSNG-RDCPJ: 523095-17 and CRSNG-RGPIN-2016-06780], and Canada Graduate Scholarships-Master's (CGS M) and Geotop Graduate Scholarships programs. Thanks to J.-F. Helie and M. Tcaci from Geotop-UQAM for the laboratory analyses. We would also like to thank four anonymous reviewers for their greatly valuable comments and edits, which helped improve the manuscript.

References

- Adomat Y, Orzechowski GH, Pelger M, Haas R, Bartak R, Nagy-Kovacs ZA, et al. New Methods for Microbiological Monitoring at Riverbank Filtration Sites. *Water* 2020; 12: 584.
- Ageos. Drinking water supply: Application for an authorization under Section 31 of Groundwater Catchment Regulation: Hydrogeological expert report. AGEOS, Brossard, QC, Canada, 2010.
- Ageos. Drinking water supply: Monitoring of piezometric fluctuations in the water table and lake levels: Period from April 27, 2012 to December 17, 2015: Annual Report 2015. 2016-928. AGEOS, Brossard, QC, Canada, 2016, pp. 42.
- Ahmed AKA, Marhaba TF. Review on river bank filtration as an in situ water treatment process. *Clean Technologies and Environmental Policy* 2017; 19: 349-359.
- Anderson MP. Heat as a Ground Water Tracer. *Groundwater* 2005; 43: 951-968.
- Ascott MJ, Lapworth DJ, Goody DC, Sage RC, Karapanos I. Impacts of extreme flooding on riverbank filtration water quality. *Sci Total Environ* 2016; 554-555: 89-101.
- Baudron P, Sprenger C, Lorenzen G, Ronghang M. Hydrogeochemical and isotopic insights into mineralization processes and groundwater recharge from an intermittent monsoon channel to an overexploited aquifer in eastern Haryana (India). *Environmental Earth Sciences* 2016; 75: 434.
- Bertelkamp C, van der Hoek JP, Schoutteten K, Hulpiou L, Vanhaecke L, Vanden Bussche J, et al. The effect of feed water dissolved organic carbon concentration and composition on organic

- micropollutant removal and microbial diversity in soil columns simulating river bank filtration. *Chemosphere* 2016; 144: 932-939B.
- Burke V, Greskowiak J, Asmuss T, Bremermann R, Taute T, Massmann G. Temperature dependent redox zonation and attenuation of wastewater-derived organic micropollutants in the hyporheic zone. *Sci Total Environ* 2014; 482-483: 53-61.
- Burnet J-B, Dinh QT, Imbeault S, Servais P, Dorner S, Prévost M. Autonomous online measurement of β -D-glucuronidase activity in surface water: is it suitable for rapid E. coli monitoring? *Water Research* 2019; 152: 241-250.
- CBC News. Ottawa River full of untreated sewage during May flooding, Ottawa, 2017.
- Centre d'Expertise Hydrique du Québec. Niveau d'eau à la station 043108 (Lac des Deux Montagnes). Ministère de l'Environnement et de la Lutte contre les Changements Climatiques, 2020.
- Clausen CH, Dimaki M, Bertelsen CV, Skands GE, Rodriguez-Trujillo R, Thomsen JD, et al. Bacteria Detection and Differentiation Using Impedance Flow Cytometry. *Sensors (Basel)* 2018; 18: 3496.
- de Sousa DN, Mozeto AA, Carneiro RL, Fadini PS. Electrical conductivity and emerging contaminant as markers of surface freshwater contamination by wastewater. *Sci Total Environ* 2014; 484: 19-26.
- Derx J, Blaschke AP, Farnleitner AH, Pang L, Bloschl G, Schijven JF. Effects of fluctuations in river water level on virus removal by bank filtration and aquifer passage--a scenario analysis. *J Contam Hydrol* 2013; 147: 34-44.
- des Tombe BF, Bakker M, Schaars F, van der Made KJ. Estimating Travel Time in Bank Filtration Systems from a Numerical Model Based on DTS Measurements. *Ground Water* 2018; 56: 288-299.
- Dillon P, Stuyfzand P, Grischek T, Lluria M, Pyne RDG, Jain RC, et al. Sixty years of global progress in managed aquifer recharge. *Hydrogeology Journal* 2019; 27: 1-30.
- Dragon K, Gorski J, Kruc R, Drozdzyński D, Grischek T. Removal of Natural Organic Matter and Organic Micropollutants during Riverbank Filtration in Krajkowo, Poland. *Water* 2018; 10: 1457.

Eckert P, Irmischer R. Over 130 years of experience with Riverbank Filtration in Düsseldorf, Germany.

Journal of Water Supply: Research and Technology - Aqua 2006; 55: 283-291.

Frey SK, Gottschall N, Wilkes G, Gregoire DS, Topp E, Pintar KD, et al. Rainfall-induced runoff from exposed streambed sediments: an important source of water pollution. J Environ Qual 2015; 44: 236-47.

Gilfedder BS, Cartwright I, Hofmann H, Frei S. Explicit Modeling of Radon-222 in HydroGeoSphere During Steady State and Dynamic Transient Storage. Ground Water 2019; 57: 36-47.

Glassmeyer ST, Furlong ET, Kolpin DW, Cahill JD, Zaugg SD, Werner SL, et al. Transport of chemical and microbial compounds from known wastewater discharges: potential for use as indicators of human fecal contamination. Environ Sci Technol 2005; 39: 5157-69.

Groeschke M, Frommen T, Winkler A, Schneider M. Sewage-Borne Ammonium at a River Bank Filtration Site in Central Delhi, India: Simplified Flow and Reactive Transport Modeling to Support Decision-Making about Water Management Strategies. Geosciences 2017; 7: 48.

Hamann E, Stuyfzand PJ, Greskowiak J, Timmer H, Massmann G. The fate of organic micropollutants during long-term/long-distance river bank filtration. Sci Total Environ 2016; 545-546: 629-40.

Hiscock KM, Grischek T. Attenuation of groundwater pollution by bank filtration. Journal of Hydrology 2002; 266: 139-144.

Hunt RJ, Coplen TB, Haas NL, Saad DA, Borchardt MA. Investigating surface water-well interaction using stable isotope ratios of water. Journal of Hydrology 2005; 302: 154-172.

Jalliffier-Verne I, Heniche M, Madoux-Humery AS, Galarneau M, Servais P, Prevost M, et al. Cumulative effects of fecal contamination from combined sewer overflows: Management for source water protection. J Environ Manage 2016; 174: 62-70.

Karakurt S, Schmid L, Hubner U, Drewes JE. Dynamics of Wastewater Effluent Contributions in Streams and Impacts on Drinking Water Supply via Riverbank Filtration in Germany-A National Reconnaissance. Environ Sci Technol 2019; 53: 6154-6161.

- Lopez-Pacheco IY, Silva-Nunez A, Salinas-Salazar C, Arevalo-Gallegos A, Lizarazo-Holguin LA, Barcelo D, et al. Anthropogenic contaminants of high concern: Existence in water resources and their adverse effects. *Sci Total Environ* 2019; 690: 1068-1088.
- Lorenzen G, Sprenger C, Taute T, Pekdeger A, Mittal A, Massmann G. Assessment of the potential for bank filtration in a water-stressed megacity (Delhi, India). *Environmental Earth Sciences* 2010; 61: 1419-1434.
- Madoux-Humery AS, Dorner S, Sauve S, Aboufadel K, Galarneau M, Servais P, et al. Temporal variability of combined sewer overflow contaminants: evaluation of wastewater micropollutants as tracers of fecal contamination. *Water Res* 2013; 47: 4370-82.
- Martin AR, Coombes PJ, Harrison TL, Hugh Dunstan R. Changes in abundance of heterotrophic and coliform bacteria resident in stored water bodies in relation to incoming bacterial loads following rain events. *J Environ Monit* 2010; 12: 255-60.
- Masoner JR, Kolpin DW, Cozzarelli IM, Barber LB, Burden DS, Foreman WT, et al. Urban Stormwater: An Overlooked Pathway of Extensive Mixed Contaminants to Surface and Groundwaters in the United States. *Environ Sci Technol* 2019; 53: 10070-10081.
- Masse-Dufresne J, Barbecot F, Baudron P, Gibson JJ. Quantifying flood-water impacts on a lake water budget via volume-dependent transient stable isotope mass balance. Accepted for public review and discussion in *HESSD* 2020: 1-30.
- Masse-Dufresne J, Baudron P, Barbecot F, Patenaude M, Pontoreau C, Proteau-Bedard F, et al. Anthropogenic and Meteorological Controls on the Origin and Quality of Water at a Bank Filtration Site in Canada. *Water* 2019; 11: 2510.
- Massmann G, Sultenfuss J, Dunnbier U, Knappe A, Taute T, Pekdeger A. Investigation of groundwater residence times during bank filtration in Berlin: multi-tracer approach. *Hydrological Processes* 2008; 22: 788-801.

- Nannou C, Ofrydopoulou A, Evgenidou E, Heath D, Heath E, Lambropoulou D. Antiviral drugs in aquatic environment and wastewater treatment plants: A review on occurrence, fate, removal and ecotoxicity. *Sci Total Environ* 2020; 699: 134322.
- Patenaude M, Baudron P, Labelle L, Masse-Dufresne J. Evaluating Bank-Filtration Occurrence in the Province of Quebec (Canada) with a GIS Approach. *Water* 2020; 12: 662.
- Ray C, Soong TW, Lian YQ, Roadcap GS. Effect of flood-induced chemical load on filtrate quality at bank filtration sites. *Journal of Hydrology* 2002; 266: 235-258.
- Reemtsma T, Berger U, Arp HP, Gallard H, Knepper TP, Neumann M, et al. Mind the Gap: Persistent and Mobile Organic Compounds-Water Contaminants That Slip Through. *Environ Sci Technol* 2016; 50: 10308-10315.
- Rose AK, Fabbro L, Kinnear S. Cyanobacteria breakthrough: Effects of *Limnothrix redekei* contamination in an artificial bank filtration on a regional water supply. *Harmful Algae* 2018; 76: 1-10.
- Sandhu C, Grischek T, Kimothi PC, Patwal P. Guidelines for flood-risk management of bank filtration schemes during monsoon in India. Saph Pani project deliverable number D1.2, 2013.
- Sandhu C, Grischek T, Musche F, Macheleidt W, Heisler A, Handschak J, et al. Measures to mitigate direct flood risks at riverbank filtration sites with a focus on India. *Sustainable Water Resources Management* 2018; 4: 237-249.
- Schwarzenbach RP, Egli T, Hofstetter TB, von Gunten U, Wehrli B. Global Water Pollution and Human Health. *Annual Review of Environment and Resources*, Vol 35 2010; 35: 109-136.
- Sjerps RMA, Vughs D, van Leerdam JA, Ter Laak TL, van Wezel AP. Data-driven prioritization of chemicals for various water types using suspect screening LC-HRMS. *Water Res* 2016; 93: 254-264.
- Snyder SA, Benotti MJ. Endocrine disruptors and pharmaceuticals: implications for water sustainability. *Water Sci Technol* 2010; 61: 145-54.
- Sprenger C, Lorenzen G, Hulshoff I, Grutzmacher G, Ronghang M, Pekdeger A. Vulnerability of bank filtration systems to climate change. *Sci Total Environ* 2011; 409: 655-63.

- Tufenkji N, Ryan JN, Elimelech M. The promise of bank filtration. *Environ Sci Technol* 2002; 36: 422A-428A.
- van Driezum IH, Chik AHS, Jakwerth S, Lindner G, Farnleitner AH, Sommer R, et al. Spatiotemporal analysis of bacterial biomass and activity to understand surface and groundwater interactions in a highly dynamic riverbank filtration system. *Sci Total Environ* 2018; 627: 450-461.
- van Driezum IH, Derx J, Oudega TJ, Zessner M, Naus FL, Saracevic E, et al. Spatiotemporal resolved sampling for the interpretation of micropollutant removal during riverbank filtration. *Sci Total Environ* 2019; 649: 212-223.
- Vogt T, Hoehn E, Schneider P, Freund A, Schirmer M, Cirpka OA. Fluctuations of electrical conductivity as a natural tracer for bank filtration in a losing stream. *Advances in Water Resources* 2010; 33: 1296-1308.
- Weiss WJ, Bouwer EJ, Aboytes R, LeChevallier MW, O'Melia CR, Le BT, et al. Riverbank filtration for control of microorganisms: results from field monitoring. *Water Res* 2005; 39: 1990-2001.
- Wett B, Jarosch H, Ingerle K. Flood induced infiltration affecting a bank filtrate well at the River Enns, Austria. *Journal of Hydrology* 2002; 266: 222-234.
- Whitehead PG, Wilby RL, Battarbee RW, Kernan M, Wade AJ. A review of the potential impacts of climate change on surface water quality. *Hydrological Sciences Journal-Journal Des Sciences Hydrologiques* 2009; 54: 101-123.
- World Health Organization. *Guidelines for drinking-water quality: fourth edition incorporating first addendum*. Geneva: World Health Organization, 2017.
- Zamyadi A, Choo F, Newcombe G, Stuetz R, Henderson RK. A review of monitoring technologies for real-time management of cyanobacteria: Recent advances and future direction. *Trac-Trends in Analytical Chemistry* 2016; 85: 83-96.

Figure 1. (a) Location of the study site and Ottawa River watershed, (b) schematic representation of the hydrogeological context and location of Lake A, Lake B and Lake DM, and (c) location of monitoring and sampling points and geological cross-section A-A'. The maps were created based on open access Geographic Information System (GIS) data. Canada's provinces boundary files were obtained from Statistics Canada © and USA Cartographic Boundary Files were retrieved from the United States Census Bureau ©. Hydrological data (lakes, streams and watershed) was sourced from the Nation Hydro Network – NHN – GeoBase Series and provided by the Strategic Policy and Results Sector of Natural Resources Canada ©. The flood extent products are derived from RADARSAT-2 images with a system developed and operated by the Strategic Policy and Results Sector of Natural Resources Canada ©.

Figure 2. Hydrogeological cross-section A-A' and location of the pumping wells and PZ-6. The screened sections of the pumping wells are located at the bottom of the aquifer. The blue and the red dashed lines represent the pre-flood and flood peak water levels at Lake A, respectively. Direct infiltration of floodwater did not occur during the intense flood events.

Figure 3. Schematic illustration of the BF system and treatment plant. The pumping wells are equipped with submersible pumps, which enable control on the active pumping wells. The pumped water flows either towards a purging system or towards the treatment plant, accordingly to the needs of the waterworks. Hand valves are open (in green) or closed (in red) to allow water to flow towards the desired direction. Sampling of the raw water can be performed at the individual pumping wells, if they are actively pumping (in blue). Typically, three pumping wells are active and contribute to the pumped mix (e.g., P6-P1-P3), which can also be sampled. The wells can also be sampled when operated in purging mode (e.g., P4 and P5). An advanced treatment and chlorination are performed on the raw pumped mix prior to its distribution to the drinking water supply system. The advanced treatment consists of biological filtration (Mangazur®) and nanofiltration (NF90 Filmtec™).

Figure 4. Temporal evolution of water levels at (a) Lake DM from 2014 to 2020, (b) Lake DM, Lake A, Lake B and PZ-4 during springtime 2017, (c) Lake DM and PZ-4 during springtime 2018 and (d) Lake DM, Lake A, Lake B and PZ-4 during springtime 2019. The black dashed line corresponds to the topographic threshold at 22.12 m.a.s.l., above which a hydraulic connection is established between Lake DM and Lake A (Ageos, 2010). On April 27, 2019, failure of a dyke (at 1 km SE to the study area) caused the flooding of a residential area, including Lake B, and resulted in rapid water level rise at Lake B (and PZ-4).

Figure 5. Spatiotemporal evolution of total bacterial counts on m-Endo media (i.e., sum of total coliform and atypical bacteria) at the pumping wells (P6, P1, P8, P2, P7, P3, P4 and P5) from January 2014 to June 2019. The data was provided by the municipal authorities. The gray shaded area represents the springtime flood events.

Figure 6. (a) Temporal evolution of electrical conductivity (EC) and $\delta^{18}\text{O}$ at the pumped mix from April to August 2019. (b) Zoom on the period between mid-April and mid-May, emphasizing the timing of the dyke failure (on April 27) and the deviation of EC and $\delta^{18}\text{O}$ from the expected curve (in red). The pumped mix was composed of groundwater abstracted at P1, P3 and P6 until April 29, after which P7 (or occasionally P8) was contributing to the pumped mix as P3 was non-operational.

Figure 7. Temporal evolution of (a) electrical conductivity (EC) and (b) $\delta^{18}\text{O}$ at the pumping wells (gray boxplots) from March 2016 to June 2019. Sample size (n) for each boxplot is normally 8 (i.e., all the pumping wells). Note that on occasional circumstances, some wells were not sampled (due to pump failure) and the boxplot were generated with $n \geq 3$ to $n \leq 7$. The gray shaded area represents the 2016, 2017, 2018 and 2019 flood events. The blue and red dashed lines correspond to the mean EC values at Lake A and Lake B (≥ 2 m depth), respectively, while the black dashed line represents the mean $\delta^{18}\text{O}$ value for floodwater. Note that the EC values at the pumping wells from March 2016 and February 2017 and the mean floodwater $\delta^{18}\text{O}$ values are retrieved from previously published work (Masse-Dufresne et al., 2020; Masse-Dufresne et al., 2019).

Figure 8. (a) Temporal evolution of the temperature at the surface of Lake A (in blue) and at PZ-6 (in black), which is an observation distant from the BF system and thus not influenced by pumping. Vertical temperature profiles on March 19, 2019 and April 25, 2019 at (b) PZ-2 and (c) PZ-5. The observation well PZ-2 is located between Lake B and the pumping well P1 (continuously pumping), while PZ-5 is near P5 (occasionally pumping).

Figure 9. (a) Daily evolution of the temperature and electrical conductivity (EC) at observation well PZ-2. The temperature measurements were performed at 11 m and 20 m depth (below ground level), while the EC measurements were only carried at 20 m depth. The frequency of bacterial analyses sampling at the pumped mix and the pumping wells is marked with black asterisks and the corresponding maximum analytical delays (i.e., 8 days) are identified with the yellow shaded areas. (b) Zoom on the period between mid-April and early May 2019, which is denoting the important transience of the temperature at 11 m and 20 m depth. Additionally, the hydraulic gradient between Lake B and PZ-2 (in red) is illustrated.

Figure 10. Evolution of $\delta^{18}\text{O}$ at the pumping wells during the recovery period in 2017. The black circles mark the wells that are contributing to the pumping mix and, therefore operating at a daily pumping rate $Q \geq 1000 \text{ m}^3/\text{day}$, while the gray circles correspond to the wells that operate at $Q < 1000 \text{ m}^3/\text{day}$. From mid-May to early August, pumping well P3 (in red) was not pumping (out of operation).

Declaration of competing interests

The authors declare that they have no known competing financial interests or personal relationships that could have appeared to influence the work reported in this paper.

The authors declare the following financial interests/personal relationships which may be considered as potential competing interests:

Journal Pre-proof

CRedit author statement

JMD, PB, FB: Conceptualization; JMD: Data curation; JMD: Formal analysis; JMD, PB: Funding acquisition; JMD: Investigation; JMD, PB, FB: Methodology; JMD, PB: Project administration; PB: Resources; PB, FB, PP: Supervision; JMD: Visualization; JMD: Writing - original draft; PB, FB, PP, BB: Writing - review & editing.

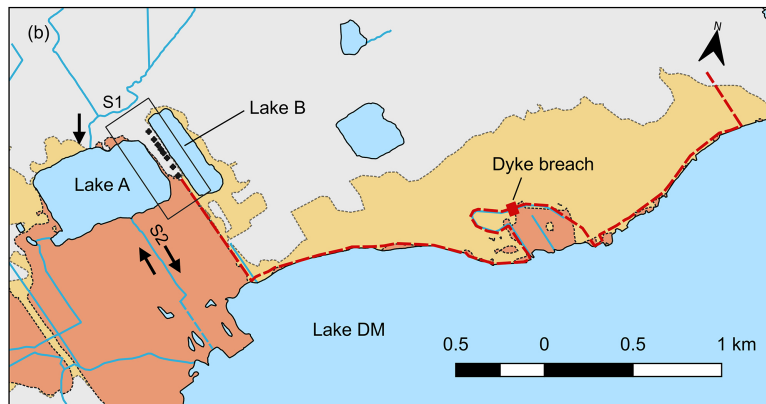
Journal Pre-proof

Graphical abstract

Highlights

- Environmental tracers are used to track the origin of bank filtrate during floods
- Groundwater flow patterns may evolve at daily timescales at bank filtration sites
- Real-time monitoring can help to anticipate potential changes in water quality
- Optimized monitoring provides insights for developing flood-adapted pumping schemes

Journal Pre-proof



Legend

- ★ Study site
- ⊕ Lake sampling point
- ⊕ Pumping well
- ⊕ Observation well
- Dyke (to prevent flooding)
- Ottawa River watershed
- Lakes
- Streams
- Flooded area
 - 2017 & 2019
 - 2019

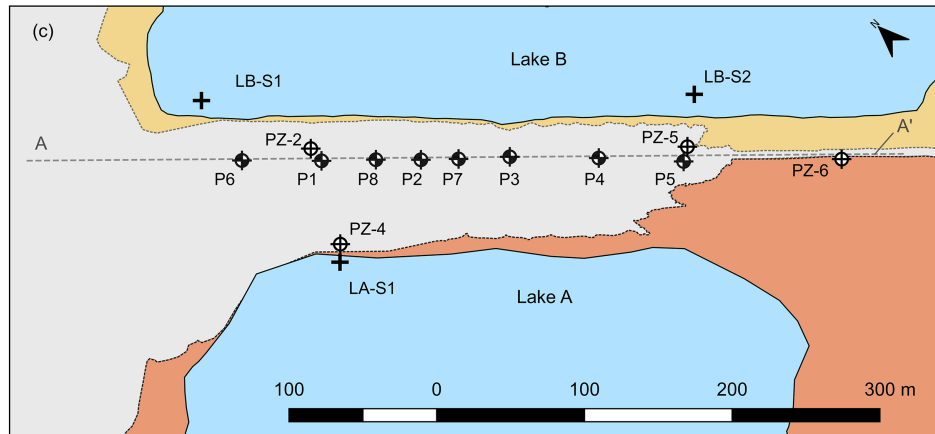


Figure 1

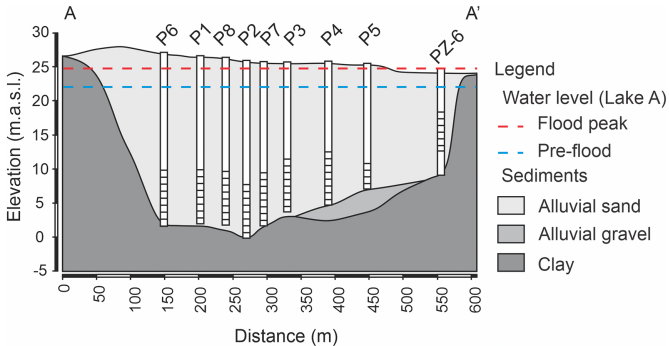


Figure 2

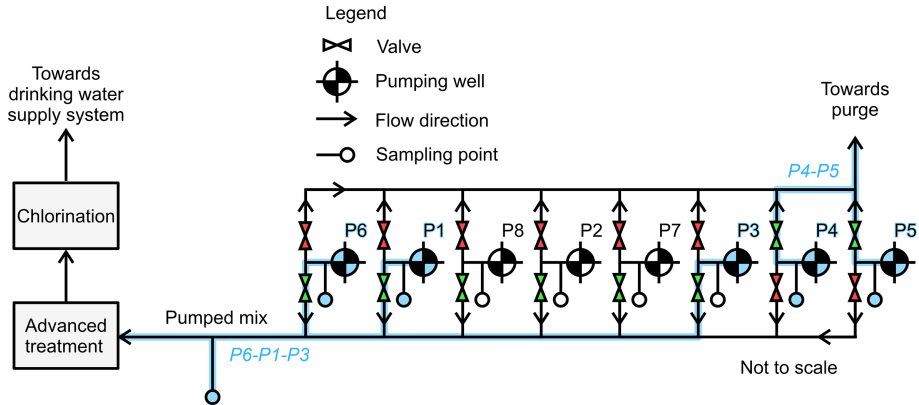


Figure 3

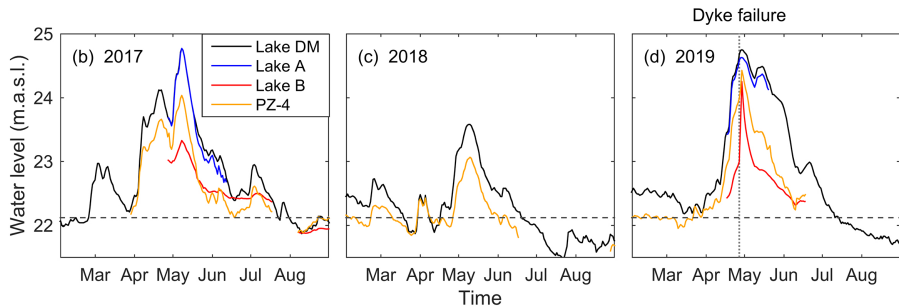
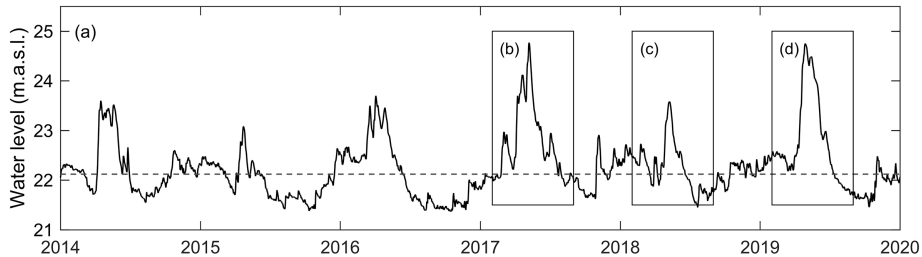


Figure 4

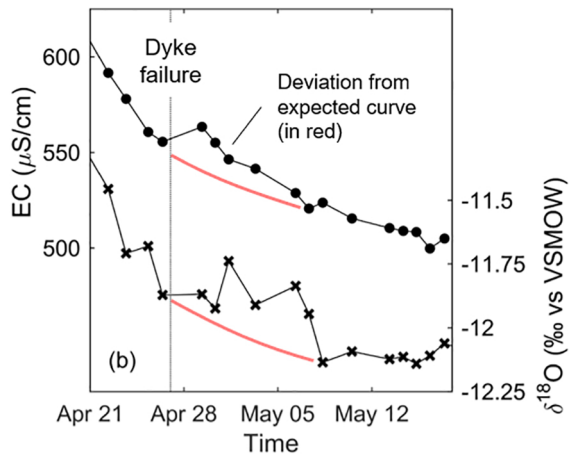
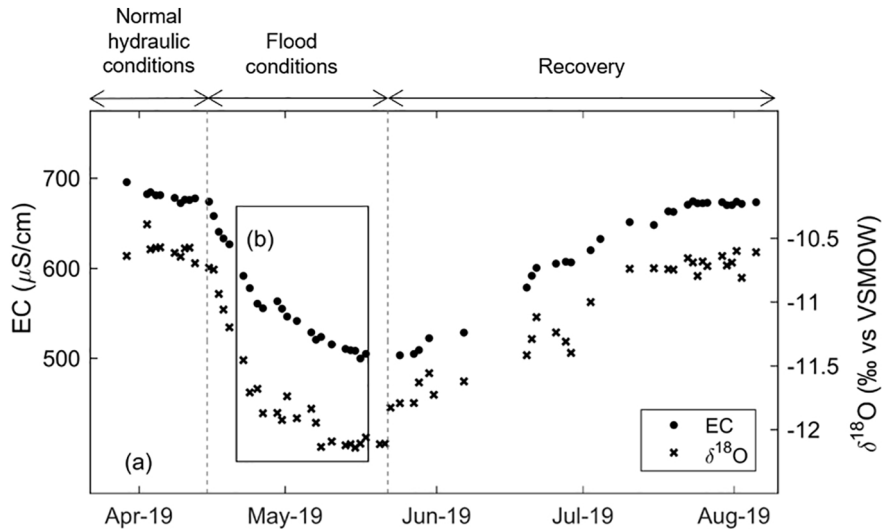


Figure 6

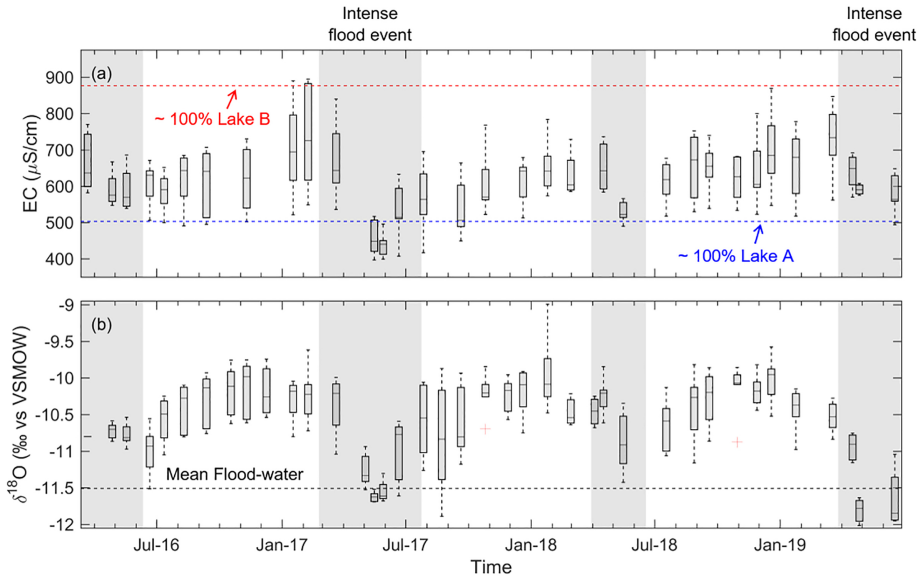


Figure 7

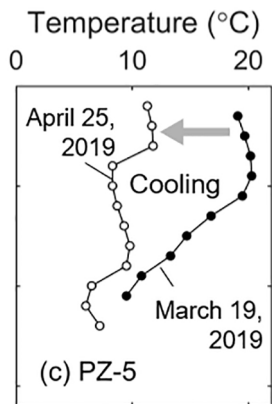
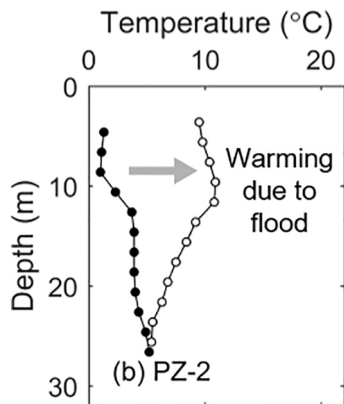
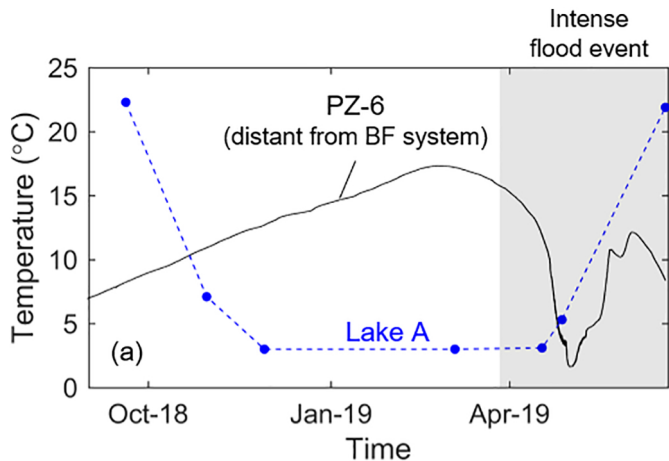


Figure 8

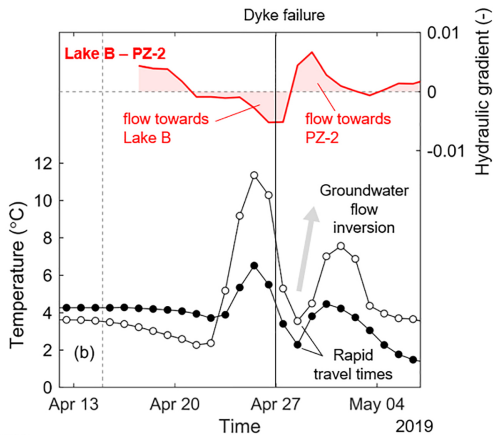
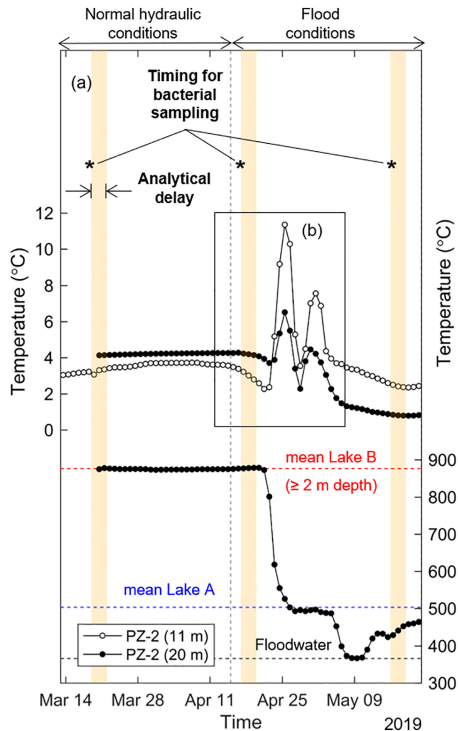


Figure 9

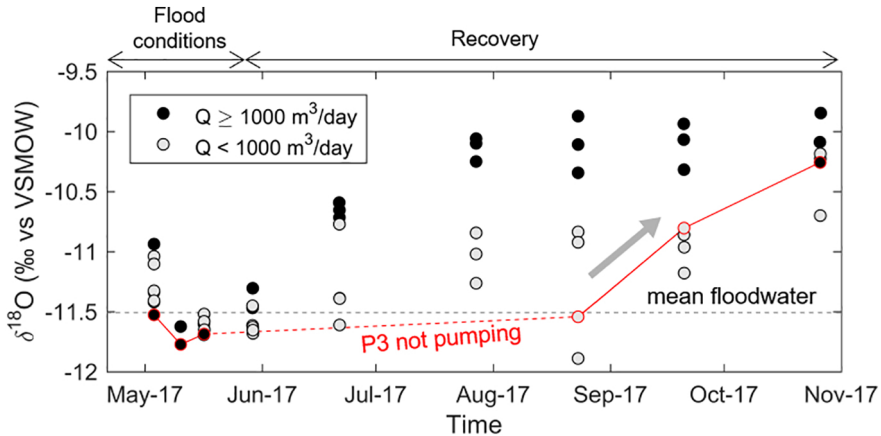


Figure 10